AIAA JOURNAL
Vol. 46, No. 12, December 2008

Control of the Shear Layer Above a Supersonic Cavity Using Energy Deposition

E. Lazar,* G. Elliott,† and N. Glumac‡
University of Illinois Urbana–Champaign, Urbana, Illinois 61801

DOI: 10.2514/1.32835

An experimental study was conducted to investigate the effectiveness of pulsed energy deposition as a means of active flow control for the shear layer above a supersonic cavity in the open configuration. The excitation pulse was generated with a Q-switched Nd:YAG laser and was applied as a spanwise oriented line along the leading edge of a cavity. The study was conducted at a freestream Mach number of 1.4 and for a cavity length-to-depth ratio of 5.29. The flowfield was analyzed over a range of delay times from the excitation laser pulse using schlieren photography and particle image velocimetry. Analysis of phase-averaged schlieren images suggested the formation and growth of a coherent large-scale structure (consisting of two adjoining vortices) in the wake of the generated disturbance. This result was confirmed through two-component velocity field data obtained from particle image velocimetry measurements. The velocity information was also used to determine the instantaneous convective velocity and define characteristic scales for the large-scale structure.

Nomenclature

a_1	=	sound speed for shear layer high-speed stream
a_2	=	sound speed for shear layer low-speed stream
D	=	cavity depth
f	=	frequency
k_c	=	ratio of convective velocity to freestream velocity
L	=	cavity length
M_c	=	convective Mach number
M_∞	=	freestream Mach number
m	=	mode number
r	=	temperature recovery factor
Sr	=	Strouhal number
St	=	Stokes number
U_c	=	convective velocity
U_1	=	shear layer high-speed stream
U_2	=	shear layer low-speed stream
U_∞	=	freestream velocity
α	=	phase delay between acoustic wave impact and vortex shedding response
γ	=	ratio of specific heats

I. Introduction

ALTHOUGH flow over a cavity represents a basic fluid dynamic configuration, this intrinsically simple arrangement can produce a number of complex flowfield characteristics (e.g., shear layer instability, flow-induced acoustic resonance, vortex flow, shock/expansion wave interaction, etc.). Consequently, the presence of these features can result in significant changes to the surroundings external and internal to the cavity, such as pressure, noise, and the convective heat transfer environment [1,2]. Although this phenomenon alone appropriately distinguishes this topic as one of fundamental interest to the discipline of fluid dynamics, the common occurrence of cavitylike geometries (e.g., wheel wells, grooves, etc.) in a wide range of tangible applications has underscored the importance of understanding its underlying physics and control. As a result, what began as a topic of scientific inquisition in the 1950s has evolved into an extensive experimental, analytical, and computational research effort [3]. Currently, two active areas of investigation in cavity flows are related to aircraft store release and combustion arrangements in proposed scramjet engines.

In supersonic aircraft, cavities are often incorporated into the vehicle design to create a weapons bay for the internal carriage of stores. This arrangement can result in a number of significant advantages, such as a reduction in aerodynamic drag and heating [4,5]. In addition, it can enhance maneuverability and generate an expanded flight envelope, improving performance and versatility [6]. However, during the release of weapons, a number of aerodynamic challenges can arise as the cavity is exposed to the freestream flowfield. These include small-scale pressure fluctuations (fundamental of turbulent shear layers) as well as acoustic resonance set up from a feedback loop within the cavity. The resulting complex unsteady flowfield can prevent store separation or even damage the store through structural vibrations. Furthermore, it can induce excessive structural loading for the aircraft, damage vital flight instrumentation, and adversely affect performance and stability [7,8]. The challenges associated with store separation have also escalated in recent years as modern weapons have become lighter (reducing inertial mass) and are being designed with more complicated geometry [9].

Additionally, cavity flowfields are also relevant to supersonic propulsion. Inherent to all scramjet engines are the challenges of fuel injection, ignition, and flame holding as parts of the combustion process in a high-speed flow. Particular difficulties are rooted in the fuel injection method, which must provide sufficient fuel–air mixing in an environment with limited flow residence time in the combustor and adverse compressibility effects [10]. Moreover, for sustained supersonic combustion, a stable region for flame holding must exist under a wide range of operating conditions. As a proposed solution, in recent years, the use of a cavity-based flame holder in the wall of a scramjet combustion chamber has been suggested as an integrated approach to overcome many of these design challenges. A cavity can optimize the mixing rate through flow recirculation, which can be enhanced by the induced periodic shedding of coherent structures into the shear layer [11,12]. The application of a cavity flowfield for improved fuel–air mixing in a scramjet engine is of particular interest to the current investigation. With this effort, results will be presented,

Presented as Paper 1229 at the 45th AIAA Aerospace Sciences Meeting and Exhibit, Reno, NV, 8–11 January 2007; received 18 June 2007; accepted for publication 4 June 2008.

*Graduate Student, Department of Mechanical Science and Engineering, 104 South Wright Street. Student Member AIAA.
†Associate Professor, Department of Aerospace Engineering, 104 South Wright Street. Associate Fellow AIAA.
‡Professor, Department of Mechanical Science and Engineering, 1206 West Green Street. Member AIAA.

demonstrating the use of pulsed energy deposition as a strategy for mixing enhancement. Specifically, it will be shown that the shear layer spanning a cavity can be optimized through the forcing of coherent structures, thereby increasing the fuel–air mixing capabilities of the flowfield.

II. Flowfield Background

A. Background

In general, a cavity flowfield can be broadly categorized into two basic flow regimes, depending primarily on its streamwise length-to-depth ratio (L/D). The significance of this parameter is revealed in its ability to predict whether the flowfield in the cavity will be in an open or closed configuration, although other transitional states may occur. A schematic illustrating both flow arrangements is shown in Fig. 1. Apparent in all flows over a cavity is the presence of a shear layer, which develops out of the boundary layer behind the leading edge of the cavity and is sustained by the velocity difference between the freestream and the flow inside the cavity. However, in the closed configuration, identified by a shallow cavity with an $L/D > 10$–13, the shear layer is unable to bridge the entire length of the cavity and rather attaches to the bottom wall before reaching the trailing edge [12]. In this configuration, the flow is generally steady and the pressure distribution along the cavity floor consists of a strong adverse gradient which can result in large drag losses, as well as being detrimental to other performance attributes, such as heat transfer [1,2]. Conversely, in the open configuration, the shear layer spans the entire length of the cavity and reattaches near the trailing edge, forming a single recirculation region below it. This type of flow is typically unsteady due to the susceptibility of instabilities in the shear layer. Consequently, for the compressible flow case, intensive noise radiation and large shock motion can develop [1]. Open cavity flows are associated with deeper cavities, identified by an $L/D < 7$–10. As with the aforementioned closed configuration, the ambiguity in the critical limits of the transition between the open to closed arrangements is due to a slight dependence on other flow parameters, including boundary-layer thickness, freestream Mach number, and cavity width [12].

A cavity in the open configuration can also exhibit either transverse (normal to the streamwise direction) or longitudinal (parallel to the streamwise direction) pressure oscillations [13]. For the case when the L/D is on the order of unity, self-sustained pressure oscillations form in the transverse mode. In short, this occurs as a result of a single vortex (formed out of shear layer instabilities) within the cavity entraining mass from the freestream and compressing the gas beneath it. This increased pressure environment ejects the vortex into the freestream flow; a new vortex is then shed from the cavity leading edge, closing the feedback loop [14]. Open cavities with an L/D approximately greater than unity oscillate in the longitudinal mode. There are primarily two similar, but distinct, models to describe the mechanism for the longitudinal oscillations. For both models, the shear layer impinging the cavity rear wall causes an inflow of freestream mass and momentum at the trailing edge. As a result, the pressure within the cavity increases and an acoustic wave develops that propagates upstream at the local sound speed. In the first model, as the acoustic wave impacts the cavity front wall, the formation of small vortices are induced at the leading edge. These vortices grow as they convect downstream, which, due to instabilities, leads to upward and downward deflections in the shear layer. In the second model, the reflection of the acoustic wave at the cavity front wall (rather than vortex shedding) causes the shear layer deflection. The feedback loop is closed when the shear layer deflection reaches the cavity trailing edge and the mass added at the beginning of the loop is ejected [12].

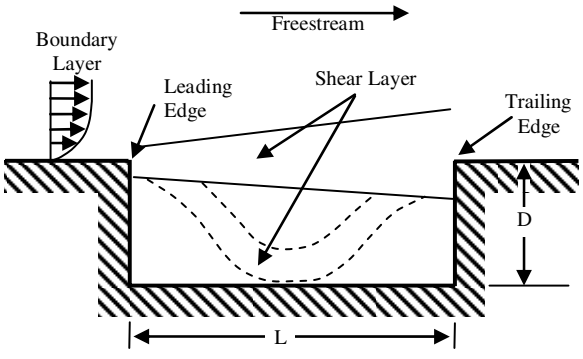

Fig. 1 Schematic of cavity flowfield operating in an open (solid line) and closed (dashed line) configuration.

The frequencies f, at which the longitudinal oscillations occur, are expressed in terms of the nondimensional Strouhal number Sr, which is based on cavity length and freestream velocity U_∞:

$$Sr = \frac{fL}{U_\infty} \tag{1}$$

The first attempt at developing a model for predicting the resonant frequencies of the cavity oscillations was undertaken by Rossiter [15] in 1964. Through experiments carried out in subsonic and transonic flows, he developed a semi-empirical equation that assumed a coupling between acoustic radiation and vortex shedding; specifically, acoustic radiation induces vortex shedding at the cavity leading edge, and the propagation of vortices over the trailing edge of the cavity causes the acoustic radiation. With these assumptions, the fluid mechanic frequency of the vortex shedding is then equal to the acoustic frequency [8]:

$$Sr_m = \frac{m - \alpha}{1/k_c + M_\infty} \tag{2}$$

where Sr_m and m are the nondimensional frequency and mode of oscillation, M_∞ is the freestream Mach number, k_c is the ratio of the convective velocity of vortices in the shear layer to the freestream velocity, and α is the phase delay between the impact of the acoustic wave at the cavity front wall and the formation of a new vortex [13]. Consequently, this semi-empirical formula allows the oscillatory mode frequencies to be calculated through a combination of empirical values for α and k_c and known values for the remaining flow parameters. However, it should be noted that, although the most commonly used values for α and k_c are 0.25 and 0.57, their universal acceptance amongst researchers is currently a topic of much debate [8,12,13]. For example, in a review of previous experimental investigations, Unalmis et al. [8] report that measurements spanning the Mach numbers of 0.4–2.5 have resulted in values of k_c ranging from 0.5 through 0.75. In addition, there are still no simple means of determining which modes will dominate and what their respective amplitude will be [13]. Rossiter's formula [15] [Eq. (2)] was also modified in 1975 by Heller and Bliss [16] such that the sound speed in the cavity would account for temperature recovery in the flow. The modified formula is as follows:

$$Sr_m = \frac{m - \alpha}{\left[M_\infty / \sqrt{1 + (r/2)(\gamma - 1)M_\infty^2}\right] + (1/k_c)} \tag{3}$$

where r is the temperature recovery factor, γ is the ratio of specific heats, and the other parameters are as described in Eq. (2).

B. Compressible Shear Layers

Compressible turbulent shear layers have also been studied independent of the cavity flowfield for a number of years. The fundamental interest in this phenomenon was originally motivated by an observed decrease in the growth rate of the shear layer with increasing Mach number as one of the freestreams becomes supersonic [13]. The first attempt at explaining this effect was by Brown and Roshko [17], who initially investigated the effect of density changes (which are present in shear layers with two different Mach numbers) by experimentally varying the density ratio across a subsonic shear layer by using two streams of different gases. As a result, they observed a first-order reduction in the growth rate of the

shear layer. In relation to high-speed flow conditions, the Mach number difference across the shear layer develops a similar density variation, and the compressibility effects directly account for a growth rate that is less than accounted for by the density variation alone [18]. The investigation by Brown and Roshko [17] also clearly revealed the presence of coherent large-scale structures that develop in the shear layer; consequently, they are often referred to as "Brown and Roshko" structures. Through this discovery and the realization that they are related to the instability of the shear layer, the idea of developing a coordinate system based on the motion of large-scale structures was later introduced by Papamoschou and Roshko [19]. Specifically, the coordinate system relates to a reference frame moving with a convective velocity U_c, defined as the velocity of dominant coherent structures. Within this convective frame of reference moving with a respective convective velocity, Papamoschou and Roshko [19] characterized a large-scale structure in the shear layer as consisting of a common stagnation point between the high- and low-speed streams. By then considering the two streamlines from each freestream, this led to the formulation of a pressure boundary condition, allowing the convective velocity to be calculated and a convective Mach number M_c to be determined. Accordingly, the convective Mach number defined by Papamoschou and Roshko [19] for two freestreams with the same specific heat ratio is given by

$$M_c = \frac{U_1 - U_c}{a_1} \tag{4}$$

and the convective velocity is given by

$$U_c = \frac{a_1 U_2 + a_2 U_1}{a_1 + a_2} \tag{5}$$

where U_1 and U_2 are the velocities of the high-speed and low-speed streams, and a_1 and a_2 are the corresponding sound speeds. However, it should be noted that modified forms of the convective Mach number have been developed to account for recompression shocks that may be present in the shear layer under high-compressibility conditions [13].

From Eq. (5), the convective velocity of the shear layer over a cavity can be calculated. Following the work of Murray and Elliott [13], which was based on earlier studies by Rossiter [15] and Heller and Bliss [16], the velocity of the fluid of the low-speed stream is neglected ($U_2 = 0$). Also, adiabatic temperature recovery was used by setting the temperature of the fluid within the cavity to be equal to the stagnation temperature. Thus, Eq. (5) yields an expression for the convective velocity ratio for the cavity flow, which is given by

$$k_c = \frac{1}{(a_1/a_2) + 1} = \left(\frac{1}{\sqrt{1 + (\gamma - 1/2)M_\infty^2}} + 1 \right)^{-1} \tag{6}$$

In the current investigation, convective velocities predicted with Eq. (6) will be compared with those from experimental results.

C. Cavity Flow Control Techniques

With a wide range of tangible applications, the practical interest of controlling the characteristics of a cavity flowfield has led to the investigation of a number of novel approaches. Although flow control techniques can be classified in several different ways, in general, two main categories exist: passive and active excitation. Passive excitation methods use a permanent change to the flowfield, either through a geometric alteration to the cavity or by a mounted obstruction in the flow. Methods within this category are typically inexpensive and simple, and can be employed through a variety of mechanisms, such as with spoilers, vortex generators, or by slanting the rear wall of the cavity to force a modification in the shear layer reattachment process [12]. Of particular interest to the current study is the application of these devices to counteract the observed decrease in the growth rate of the shear layer with increasing compressibility. In experiments performed by Island et al. [20], boundary-layer disturbances were introduced by applying small pieces of Scotch tape to the high-speed (supersonic) side of a splitter tip. Different geometric parameters for the disturbances were also investigated, which included changing their shape, number used, spatial distribution and location, surface texture, and thickness. Planar laser Mie scattering images and schlieren photography demonstrated that discrete three-dimensional disturbances increased the near- and far-field growth rate, with enhancements of up to 45%. This was also presented with quantitative mixing measurements using cold chemistry planar laser-induced fluorescence. Results from this diagnostic revealed up to a 7% increase in the mixing efficiency. When coupled with the increased thickness of the shear layer, this led to about 57% more mixed fluid than for the unperturbed case at the same compressibility. However, although this study, as well as many others, has demonstrated the effectiveness of passive excitation methods, because these devices are permanent features, they are generally limited as they typically can only be optimized for a specific flow condition. Consequently, performance can degrade to conditions worse than for the unforced case [21].

In contrast, active excitation methods can continuously change and adapt to different flow conditions. Broadly speaking, forcing techniques of this type include acoustic driving, mechanical excitation, and fluid injection methods [22]. In relevance to cavity flowfields, the use of steady or pulsating microjets has acquired particular interest as a means of active flow control. In addition to being effective at controlling the cavity oscillations, this technique is advantageous as it is small, robust, and capable of producing a high momentum flux with a very small mass flux [3]. As an experimental example, Zhuang et al. [23] investigated the use of supersonic microjets at the leading edge of a Mach 2 cavity with an $L/D = 5.19$. The study concluded that the activation of the microjets resulted in up to a 20 dB reduction of amplitudes in cavity tones and more than 9 dB in the overall sound pressure levels. The injected mass also led to modifications in the shear layer and a significant reduction of the flow unsteadiness inside the cavity. There have also been a number of computational investigations. Rizzetta and Visbal [7] numerically studied the application of high-frequency (5 kHz) forcing through pulsed mass injection at the leading edge of a cavity with an $L/D = 5$ and at Mach 1.19 to investigate the ability of large-eddy simulations to predict acoustic resonance suppression. They found that the perturbed shear layer resulted in several changes in comparison with the unforced case, including acoustic suppression, altered characteristics of vortices, and a decreased amplitude of vertical shear layer deflections.

While these types of mechanical devices have shown to be effective, there are several disadvantages associated with them. In particular, with devices such as blowing/suction jets, there are inherent challenges with installation and concerns about reliability and performance under extreme conditions such as icing or trapped debris [24]. Accordingly, in recent years, there has been a renewed interest in the use of energy deposition for high-speed flow control. The scope of this research activity encompasses a wide range of approaches (e.g., plasma arcs, pulsed lasers, microwaves) for use in practical applications, including drag reduction, lift and moment enhancement, and in forcing modifications to shock structures [22,25]. A selective review of using energy deposition as a means of aerodynamic flow control at high-speed is given by Knight [25]. In a related computational study, Aradag et al. [6] numerically examined the use of pulsed energy deposition to reduce the resonant pressure fluctuations in a cavity with an $L/D = 5.07$ and at Mach 1.5. A periodic pulsed input of 1.0 mJ was applied to the leading edge of the cavity to simulate energy deposition by a laser. The input was added at the beginning of each fundamental Rossiter period. Their simulation indicated that the applied forcing induced a reduction of the pressure fluctuations for the first several Rossiter modes, changing the flow structure within the cavity.

In the present experimental investigation, energy deposition will be similarly introduced to the leading edge of a supersonic cavity through the use of a pulsed laser. However, the forcing will be applied at a relatively low frequency of 10 Hz to provide a single burst of excitation to the shear layer spanning a cavity. The effectiveness of this technique will be determined by its ability to

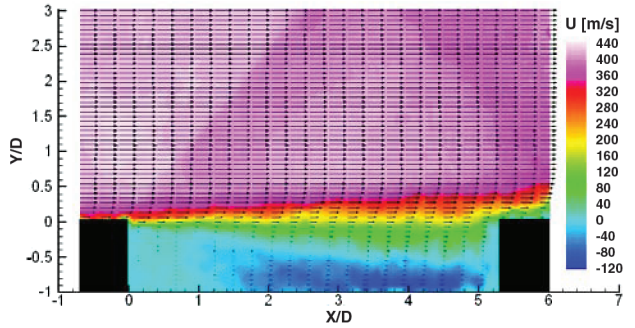

Fig. 2 Streamwise velocity profile of entire cavity flowfield obtained with PIV data.

enhance the large-scale structures that develop in the shear layer to improve fuel–air mixing capabilities of scramjet engines. This experimental investigation is part of an ongoing joint research program with research colleagues at Rutgers University who have previously reported on computer modeling efforts for this type of flowfield [6].

II. Experimental Setup

A. Wind-Tunnel and Flow Conditions

In the current experimental study, the flow over a rectangular cavity was investigated using a supersonic blowdown wind tunnel. The tunnel was operated with good flow quality (i.e., in the absence of strong compression or expansion waves in the test section) at a Mach number of 1.4. The flowfield conditions were confirmed with ensemble averaged velocity measurements obtained from particle image velocimetry (PIV) data. An illustration of the streamwise velocity for the unforced flowfield is shown in Fig. 2. Air was supplied through an Ingersoll–Rand compressor with a volumetric flow rate of 2040 m^3/s and at a pressure of 1000 kPa. The flow from the compressor was filtered, dried, and cooled, and traveled to a 140 m^3 tank farm. From this point, the air travels through a pipe to a pneumatic valve controlled by a Fisher TL 101 process controller and a manual gate valve before entering the wind tunnel. Before reaching the test section, the flow passes through a conventionally arranged settling chamber with a honeycomb filter and subsequent screens to reduce the scale of the incoming turbulence and to straighten and make the flow uniform. The cavity was located in the top wall of the wind-tunnel test section, which has a square cross section measuring 63.5 mm on each side. The dimensions of the cavity were 71.9 mm long × 13.6 mm deep ($L/D = 5.29$) and spanned across the width of the test section. This arrangement forces the flowfield in the cavity to be in the open configuration and creates longitudinal oscillations for experimental investigation. There are also large windows on each side of the test section to allow flow visualization studies to be conducted and a smaller window on the bottom to provide access for energy deposition into the flowfield [26]. A full description of the wind tunnel can be found in [26]. Relevant flow condition parameters have also been summarized in Table 1. In Table 1, the convective Mach number was calculated with Eqs. (4) and (6), which represents adiabatic temperature recovery in the cavity as used by other researchers [13]. For comparison, the convective Mach number was also calculated with the most commonly used value for temperature recovery, $r = 0.89$ [8]. Under this condition, the value varied only slightly with $M_c = 0.65$.

Table 1 Summary of experimental test condition

Stagnation pressure	200–235 kPa
Stagnation temperature	27–34°C
Boundary-layer thickness [26]	6.58 ± 0.1 mm
Cavity length	71.9 mm
Cavity depth	13.6 mm
Freestream Mach number	1.4
Convective Mach number	0.64

B. Forcing Laser Setup

As a means of controlling the growth rate of coherent structures in the shear layer, pulsed energy deposition from a Quantel Brilliant series Q-switched Nd:YAG laser was used as a form of excitation. The laser was operated at a wavelength of 532 nm, delivering approximately 230 mJ per pulse at a frequency of 10 Hz. The energy generated from the laser pulse was focused using a spherical lens and then expanded along the width of the cavity leading edge using a cylindrical lens. This optical arrangement resulted in a focused 25 mm spanwise oriented "line" defining the excitation region. As a result, a single burst of excitation was introduced and ionized the flow before it propagated the length of the cavity.

Results from linear stability analysis and experimental measurements/observations indicate that, for a compressible planar shear layer, as the convective Mach number increases, the flow becomes more three-dimensional and the most amplified waves are oblique for convective Mach numbers above 0.6 [27,28]. This rise in the three-dimensionality is important, as it may impact the ability to force and control compressible mixing layers [29]. However, Murray and Elliott [13] suggest that, for cavity flows, the presence of two-dimensional structures in the shear layer persists at higher Mach numbers (freestream Mach numbers up to 2.1). Also, from linear stability theory, Sandham and Reynolds [28] showed that, in the convective Mach number range of the current study (~0.7), the most amplified wave may be oblique (at approximately 31 deg according to their formula), but the amplification appears to be relatively flat for lower disturbance angles based on their plot of amplification. Additionally, based on our previous studies of flow control of shear layers using energy deposition for jets exhausting into ambient conditions, it was found that positions near the exit (corner between the high-speed flow and ambient) provide an excellent and possibly optimal position for excitation [22]. Therefore, for the current study, the location of the excitation pulse in the corner of the cavity was used and, coupled with the geometry of the cavity, restricted the study to using 2-D forcing.

C. Flowfield Diagnostics

The resulting flowfield was analyzed with a standard *Z*-arrangement schlieren system. Illumination was provided by a xenon spark lamp, which acted as a point light source providing high luminance and emitting a continuous spectrum of light, ranging from ultraviolet through visible to infrared. The generated light was then collimated through the wind-tunnel test section and then focused to a point. Instantaneous schlieren images were recorded in the vertical and horizontal knife-edge configuration with a 1600 × 1200 pixel charge-coupled device (CCD) camera. The duration of each flash was on the order of 20 ns and an imaging exposure time was set at 1 μs, which resulted in conditions short enough to freeze most of the turbulent structures and produce instantaneous images of flow [23]. All equipment was controlled with an eight-channel Quantum Composer pulse generator. A top-down view of the experimental schlieren setup is shown in Fig. 3a.

In addition, two-dimensional PIV measurements were conducted to obtain quantitative velocity fluctuation data. A schematic of the experimental setup used for obtaining the PIV images is shown in Fig. 3b. The main flow was seeded with diethylhexyl sebacate (DEHS) though the use of a Laskin nozzle that generated particles with a diameter less than 1 μm [30]. The seeding was introduced approximately 3.5 m upstream of the test section, which resulted in a sufficient dispersion of the particles into the cavity and the freestream flow. The particles were illuminated by a thin (on the order of 0.1 mm) light sheet that spanned the streamwise length of the cavity at approximately the middle of the test section width. The light sheet was created by a dual-head New Wave Nd:YAG laser in conjunction with spherical and cylindrical lenses. The PIV laser was operated at a frequency of 532 nm, with each pulse delivering approximately 40 mJ of energy. To avoid saturation of the CCD from intense

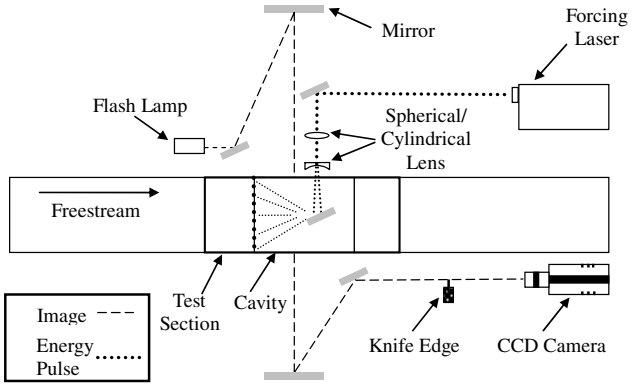

a)

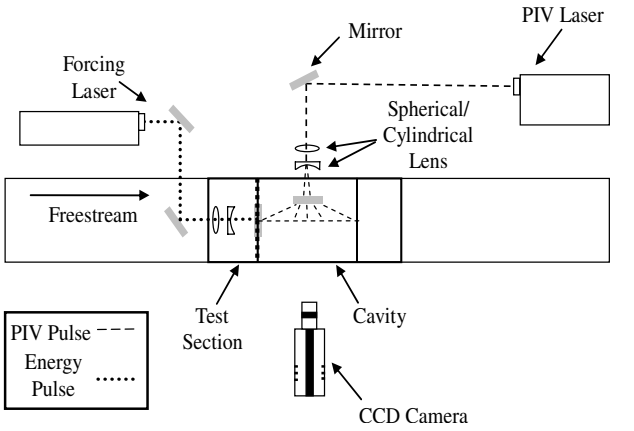

b)

Fig. 3 Schematic of flow visualization setups: a) schlieren and b) PIV.

reflections, the cavity surface was painted with a rhodamine-based fluorescent paint. As a consequence (with about 30% efficiency), the wavelength of the light off of the cavity walls was increased from 532 nm to above 620 nm. By using a 532 nm bandpass filter on the camera, this allowed the particle signal to be picked up closer to the cavity walls. The time separation between the laser pulses to illuminate the DEHS particles was adjusted according to the flow velocity and camera magnification. The PIV images recorded were taken with the CCD camera as described previously in the schlieren photography setup. The image pairs for each delay time and for the no-forcing case were then processed and averaged through a PIV program developed by Innovative Science Solutions, Inc.

The accuracy of velocity measurements obtained from the PIV data was a composite of the ability of the seed to follow the flow and for the imaging and analysis system to record and process a field of particle images [31]. In quantifying the accuracy, a number of factors need to be considered, such as the number of samples, turbulence intensity, computational algorithm, equipment, and particle size [23]. The error in timing between two laser pulses was estimated to be 6 ns. The uncertainty in pixel displacement by correlation analysis of the PIV software program was approximated at one-tenth of a pixel, assuming the laser sheet is providing Gaussian illumination. Subpixel accuracy was achieved by matching the intensity captured from illuminated particles through a Gaussian shaped peak locator [32]. With these assumptions and using an ensemble average of 340 image pairs, a relative error of 2.5% was calculated for the mean velocity. For the freestream flow, the PIV measurements were less than 2% of the values predicted with 1-D gas dynamic equations. A similar comparison of measured and expected values for velocities within the cavity and shear layer could not be evaluated because these values were not known a priori [23]. Also, consideration of seed-particle dynamics was especially important because the large-velocity gradients present challenge the flow-following capability of all but the smallest particles, and spatial variations in density make it difficult to establish uniformly satisfactory seeding levels. Particle dynamic effects are typically parameterized by the Stokes number St, which is the ratio of the characteristic particle time to the time scale of the flow variations to be measured [31]. Following the work of Scarano and van Oudheusden [33], given the relatively low Mach and Reynolds numbers for this study, the drag relation suggested by Melling [34] was used to determine the characteristic particle time. The flow time scale in the shear layer was calculated from the work of Samimy and Lele [35]. This yielded, immediately downstream of separation, a worst-case Strokes number of $St = 0.024$. The response of the particles to turbulent fluctuations in the shear layer was then quantified using the results from Samimy and Lele [35], which predicted a maximum rms velocity fluctuation error, due to particle lag of approximately 0.35% [36]. Further downstream, the growth in the shear layer thickness drops the Stokes number below 0.013, reducing the particle lag error to 0.1%.

IV. Results

A. Schlieren Images

Instantaneous schlieren images were obtained to investigate the distribution of density gradients within the cavity flowfield before and after excitation. The experimental study was conducted at incremental delay times ranging from 10–1000 μs ($\pm$1 ns) from the laser energy input at the cavity leading edge. At each delay time and for the no-forcing case, 138 instantaneous images were collected and phase averaged. Although the cavity flowfield was investigated with the knife edge in the horizontal and vertical arrangements, only images in the vertical orientation are presented. The images in the vertical arrangement were selected because of the suppression of the vertical density gradients due to the shear layer and boundary layer. As a result, large-scale structures within the shear layer are more easily visualized [13].

Shown in Fig. 4, phase-averaged schlieren images are illustrated for selected delay times from the excitation pulse and also without any forcing. The direction of the flow is from left to right. Apparent in all the images, an oblique shock can be seen at the leading edge of the cavity. An expansion or compression wave is similarly seen at the trailing edge. The images also resolve the reflection of the leading-edge shock off of the bottom wall of the test section and its subsequent impact with the trailing-edge wave. Several other weaker waves can also be identified. These were formed from minor surface discontinuities in the test section walls and are common in most supersonic wind-tunnel facilities. Their presence did not appear to influence the results presented in any significant manner.

In Fig. 4a, the flowfield is shown without any applied excitation. As discussed earlier, the dynamics of cavity flowfields are dominated by a feedback mechanism, consisting of instability waves or shear layer structures in one leg and acoustic waves on the return [23]. Therefore, although dominant cavity tones were expected, the phase-conditioned data were not measured with respect to them. Accordingly, in Fig. 4a, no large-scale structures are evident due to their decreased coherence and random occurrence. Fig. 4b corresponds to a 10 μs delay from the excitation pulse. In this image, the blast wave from the laser pulse originates at the leading edge and is distorted by the relative velocity internal and external to the cavity. At this point, the disturbance has not significantly propagated through the flow and the shear layer remains primarily unaltered. In Figs. 4c and 4d, the delay time between excitation and imaging was increased to 20 and 40 μs, respectively. At these increased times, the disturbance from the laser pulse, which first appeared as a single thermal spot, has traversed through the shear layer to considerably alter the flowfield. Specifically, in image Fig. 4c, a neighboring pair of light and dark regions (centered approximately in the wake of the blast wave) can be identified. A second similar pair of regions can also be seen forming in the shear layer image in Fig. 4d. Although the schlieren images provide no further qualitative information toward the nature of these induced regions, the shadow pattern suggested a density variation distribution and location that was consistent with the presence of a large-scale structure within the shear layer. Further discussion will be given

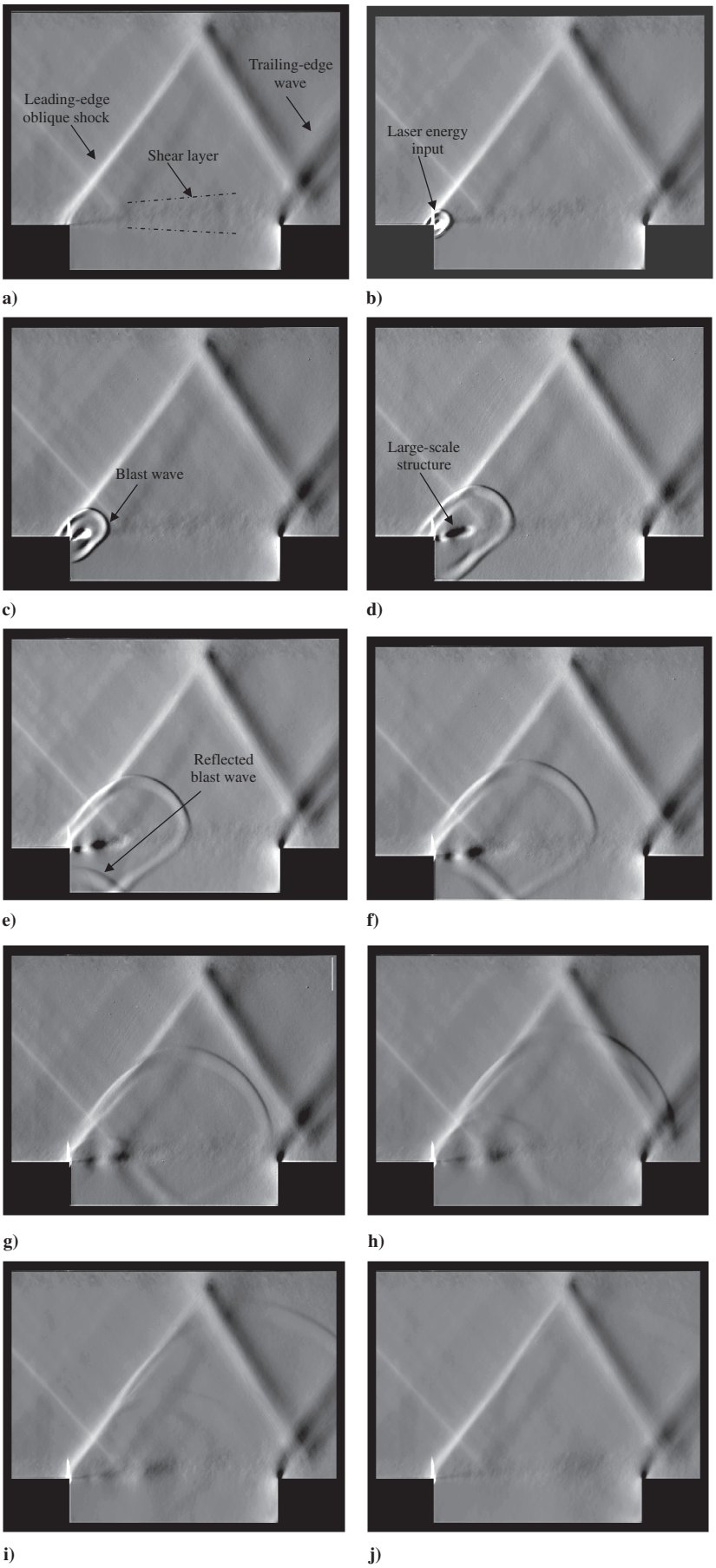

Fig. 4 Phase-averaged schlieren images a) without forcing, and at selected delay times from an energy input: b) 10 μs, c) 20 μs, d) 40 μs, e) 60 μs, f) 80 μs, g) 100 μs, h) 120 μs, i) 160 μs, and j) 240 μs.

using two-component velocity field measurements obtained using PIV. Through the velocity data, it will be shown that the structure consists of two vortices with a common stagnation point between them, therefore having a comparable appearance and behavior to the model proposed by Papamoschou and Roshko [19]. Shown in Figs. 4e–4j for increasing delay times, the large-scale structure (both proposed vortices) convects, grows, and decays as it moves further downstream.

In addition to the formation of the large-scale structure in the shear layer, the images in Fig. 4 also illustrate the propagation of the blast wave through the cavity flowfield. Associated with this event is the reflection of the blast wave off of the cavity bottom wall, which results in a reflected wave, forming a second disturbance to the shear layer. The reflected wave can first be seen in Fig. 4e. In this image, 60 μs have elapsed from the energy input and the reflected wave is propagating toward the underside of the shear layer. The resulting impact is shown in Figs. 4f–4h. In contrast to the initial wave, the reflected wave appeared to transverse through the shear layer while leaving it primarily unaltered. Although this phenomenon was not directly investigated, Figs. 4f–4h suggest three possible explanations. First, with increasing time, the energy of the blast wave is distributed over a greater arc length and dissipated by flowfield motions, reducing its local intensity. As a result, the reflected wave may have been too weak to provide a sufficient disturbance to alter the shear layer. Secondly, the reflected wave obliquely impacts the bottom of the shear layer and then propagates across its thickness. This differs from the initial wave that spans the entire shear layer thickness and transverses along its length. Lastly, as shown in Figs. 4f–4h, the reflected wave impacts the section of the shear layer containing the large-scale structure. Although the interaction between these features is not clear, the presence of the structure may have suppressed any affects from the reflected wave.

B. Particle Image Velocimetry

PIV was conducted to determine the two-component velocity field and provide quantitative information on the large-scale structure that formed in the shear layer from the energy deposition at the cavity leading edge. Ensemble averages of 340 image pairs were used for the analysis of all conditions tested. The results are presented as color contours for the average transverse and streamwise velocity components and for a selected region of the cavity flowfield. This region was chosen to show key attributes of the flow, which included the propagation of the blast wave through the shear layer and the subsequent formation and development of the large-scale structure. For all of the velocity data presented, the axes of the images were nondimensionalized by the cavity depth. Also, for streamwise locations, the selected view was positioned such that the full length of the x axis directly corresponds to the full cavity length. Consequently, the upstream wall of the cavity is located at $X/D = 0$, whereas the downstream wall is at $X/D = 5.29$. Along the y axis, negative values of Y/D identify locations within the cavity, whereas positive values are those within the freestream. Therefore, using a conventional format for coordinates $(X/D, Y/D)$, the cavity leading edge is located at (0, 0), the cavity trailing edge at (5.29, 0), and the cavity bottom wall for all values of X/D with $Y/D = -1$.

1. Transverse Velocity Component

In Fig. 5, the average transverse velocities are shown for selected delay times from the energy input, ranging from 40 to 240 μs (± 1 ns) and also without excitation. Apparent in all of the images of Fig. 5, the leading-edge oblique shock can be identified as a velocity field boundary in the upper left corner. The shear layer is also shown by the region of decreased transverse velocity along the streamwise direction for $Y/D = 0$. A baseline illustration of the flowfield without any forcing applied is shown in Fig. 5a. Consistent with the phase-averaged schlieren images, no organized motions within the shear layer can be identified.

In Fig. 5b, 40 μs have elapsed from the excitation pulse. The resulting blast wave is shown by the band of sharp velocity change that is approximately centered about the cavity leading edge [i.e., $(X/D, Y/D) = (0, 0)$]. In the wake of the blast wave, induced vertical motions in the flowfield (internal and external to the cavity) can be seen. These vertical motions are especially significant in the wake of the blast wave entering the cavity. The initial development of the large-scale structure illustrated in the schlieren images can also be seen forming in Fig. 5b at the cavity leading edge. In this case, the structure is first identified as a coherent region of increased positive transverse velocity; for clarity, this region is boxed in dashed lines in Fig. 5b. In Fig. 5c, 80 μs have elapsed from the energy input. At this delay time, the boxed region of positive transverse velocity identified in Fig. 5b has propagated away from the cavity leading edge and undergone considerable growth. Additionally, a second region of negative transverse velocity can be seen forming at the upstream end of the image. Fig. 5c also illustrates the development of the reflected blast wave within the cavity. The flowfield following its impact with the reflected wave and shear layer is shown in Fig. 5d. The full development of the large-scale structure can be seen in Fig. 5e, which corresponds to a delay time of 160 μs. In this image, four regions of transverse velocity, alternating between positive and negative, can be observed; collectively, these four regions are referred to as the large-scale structure seen in the schlieren images. The four regions have also been labeled (I, II, III, and IV) in image Fig. 5e, and this convention will be referred back to throughout the discussion.

By comparing Figs. 5b–5e, it can be seen that, although region I was partially visible at all delay times, it did not become well defined until Fig. 5e, which was for 160 μs. Furthermore, in Fig. 5e, region II appears to have undergone a similar transition and is also positioned relatively high in the shear layer. It is unclear if this result was due to the impact of the reflected blast wave with the shear layer or the manner in which it would have naturally developed. In further defining the large-scale structure, the alternating directions of the neighboring velocity field regions (I–IV) suggested the presence of vortices within the shear layer. In particular, it is proposed that the pair of regions I and II and regions III and IV each represent a vortex, where then both vortices represent the large-scale structure. Taking after Adrian et al. [37], although a widely accepted definition of a vortex does not exist in the fluid dynamics community, for the present study, the definition offered by Kline and Robinson [38] is used: "A vortex exists when instantaneous streamlines mapped onto a plane normal to the core exhibit a roughly circular or spiral pattern, when viewed in a reference frame moving with the center of the vortex core." Accordingly, two necessary conditions are that the velocity field must be viewed in a convective reference frame and that the vorticity must be concentrated in a "core." If a turbulent field consists of large-scale motion with many small-scale vortices embedded within it, it will only be possible to identify a vortex in terms of the foregoing definition if the velocity at the center of each small vortex is removed [37]. From this method, the respective streamlines for the flowfield were analyzed in a convective reference frame. This was completed by subtracting the experimental convective velocity for the streamwise velocity measurements from the PIV data. The resulting streamlines are shown in Fig. 6, where they have been superimposed on the transverse velocity contours at a delay time of 160 μs. The streamwise axis has also been reconfigured with the stagnation point, so that the scale of each vortex can be clearly seen. Shown in this representation, two vortices are clearly identifiable with a stagnation point between them. Although similar types of structures periodically form in cavity flowfields due to a feedback mechanism, where the modal frequency is given by Eqs. (2) or (3), Fig. 6 illustrates the effectiveness of the excitation pulse to interact with the dominant instabilities of the undisturbed cavity flow.

2. Streamwise Velocity Component

As the counterpart to the transverse velocity images, similar analysis for the average streamwise component was also determined. The resulting velocity contours are shown in Fig. 7. In Fig. 7a, the flowfield is shown without any excitation applied. The leading-edge oblique shock can be identified as a velocity boundary in the upper left corner, where there is a slight velocity decrease downstream of

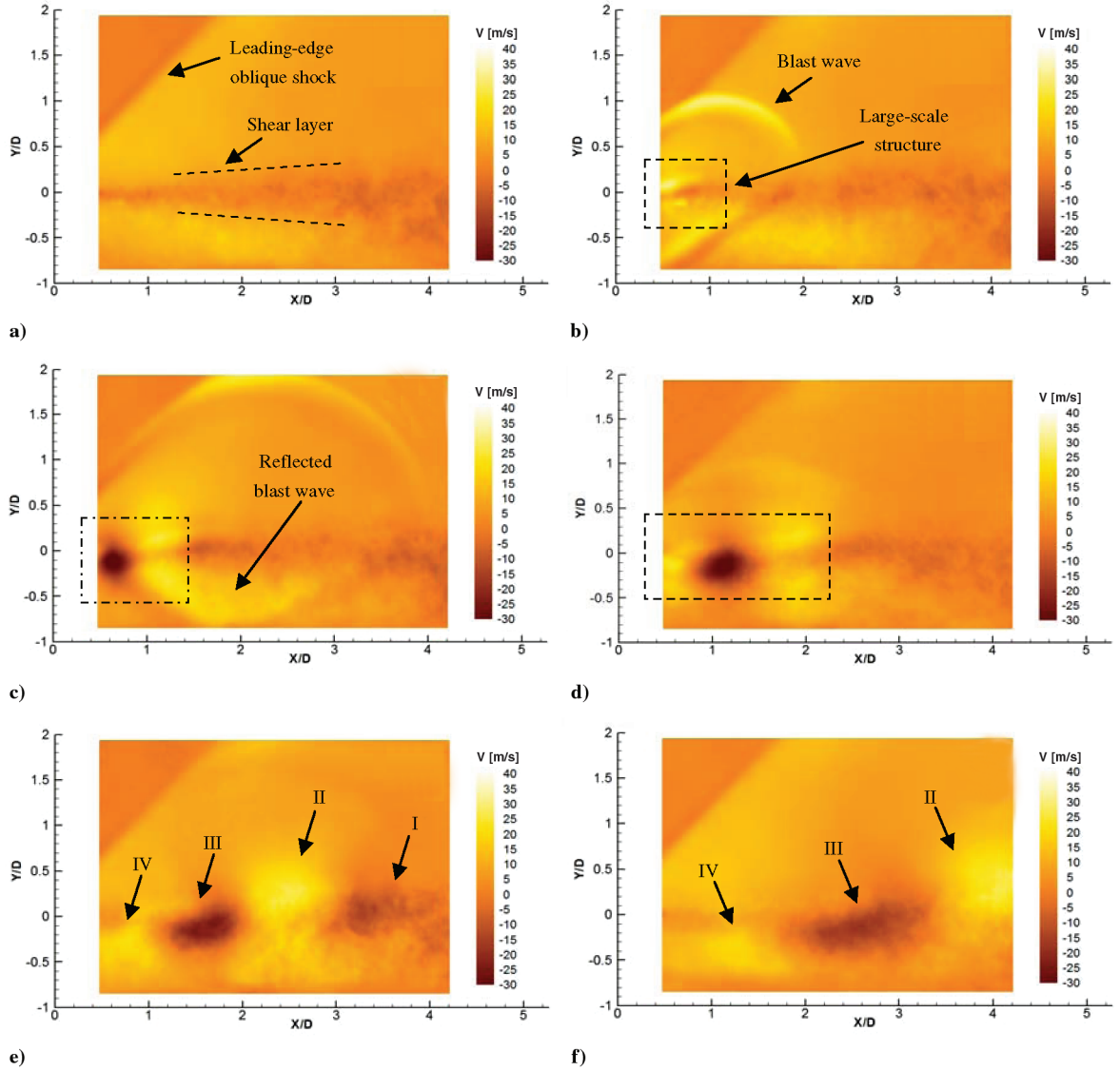

Fig. 5 Average transverse velocity a) without forcing, and at selected delay times from an energy input: b) 40 μs, c) 80 μs, d) 120 μs, e) 160 μs, and f) 240 μs.

the shock. Within the cavity, negative streamwise velocities are resolved representing a recirculation region, fundamental of open cavity flows. Velocity data from Fig. 7a also reveal that the reverse velocities within the cavity reach as high as 25% of the freestream value ($\sim$100 m/s). However, higher reverse velocities may exist outside of the region shown in Fig. 7a. For increased values of Y/D, the recirculation region diminishes with the flow velocity eventually becoming stagnant and then positive, representing the lower boundary of the shear layer. Within the shear layer, the streamwise velocity progressively transitions from supersonic conditions to stagnant over a distance ranging from approximately 6.1 mm at the leading edge to 11.6 mm at the trailing edge ($\pm$0.03 mm for both measurements based on the spatial resolution of the images and the error in the mean velocity). These values were based on spatial measurements of 5 and 95% of the freestream velocity. Although for this type of flow there were significant reverse velocities within the cavity, the recirculation region was not well defined along its streamwise length and especially at the leading and trailing edges where the shear layer thickness was estimated. Accordingly, the convention used for defining the shear layer thickness is assumed appropriate for establishing the comparative trends in the present study.

In Fig. 7b, 40 μs have elapsed from the excitation pulse. Although the blast wave is less apparent than the images of the transverse component in Fig. 5, it can be recognized as a curved region of slightly increased streamwise velocity approximately centered about the cavity leading edge. The location of the large-scale structure is also less defined. However, as seen in Figs. 7c–7f, as the large-scale structure convects downstream, it causes a slight thickening of the shear layer. This also leads to a deflection in the upper and lower boundaries defining the shear layer, as highlighted in Figs. 7c and 7d. By comparing the location of the deflection with the images of the

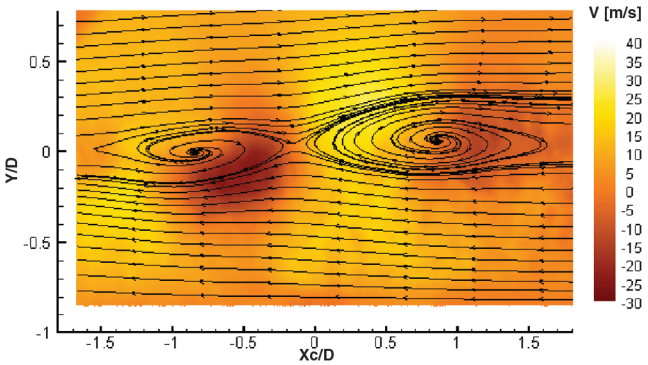

Fig. 6 Transverse velocity contours at a 160 μs from the excitation pulse with superimposed streamlines analyzed in a convective reference frame.

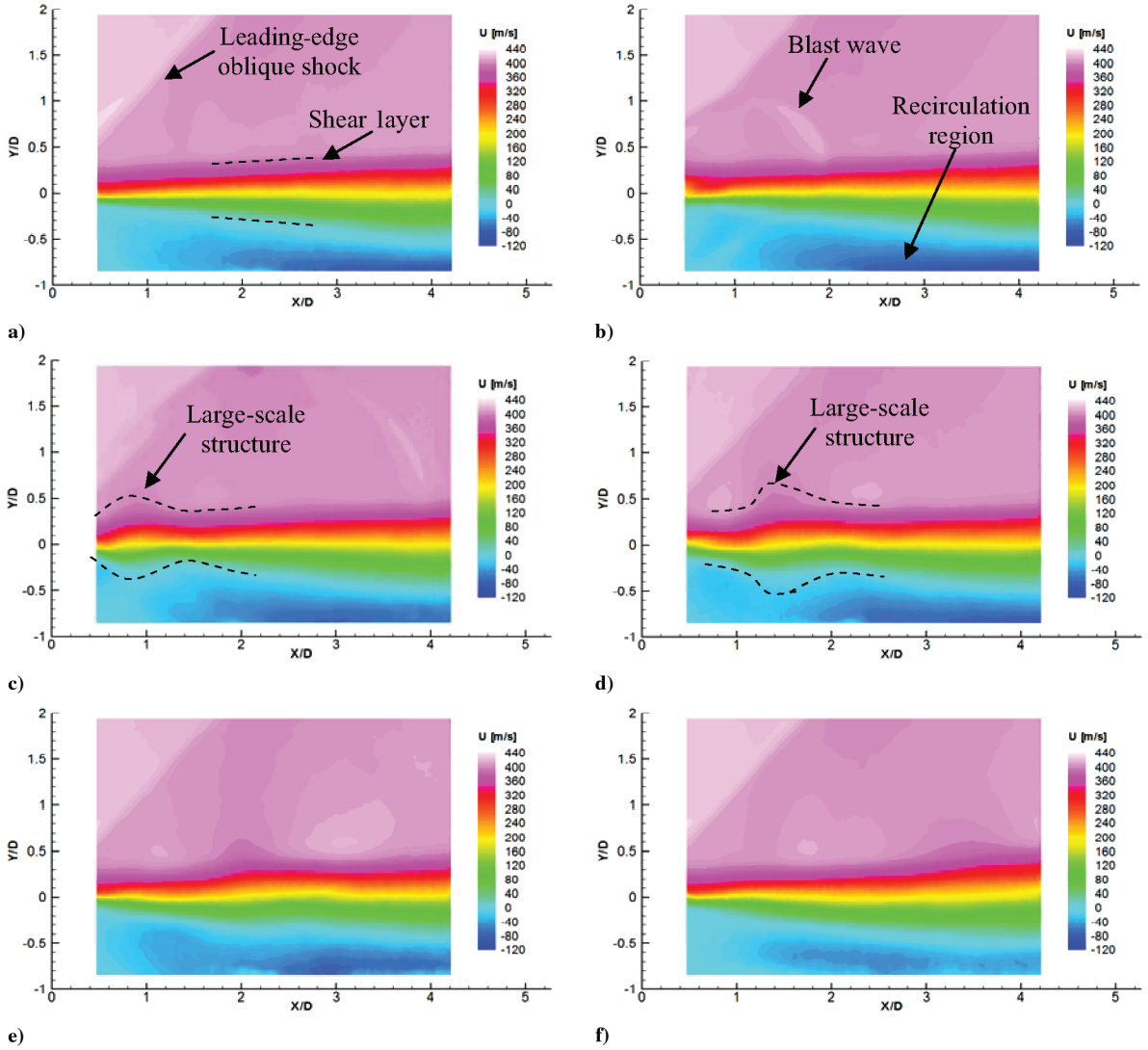

Fig. 7 Average streamwise velocity a) without forcing, and at selected delay times from an energy input: b) 40 μs, c) 80 μs, d) 120 μs, e) 160 μs, and f) 240 μs.

transverse velocity component, its position is approximately the same as the stagnation point between the two vortices shown in Fig. 6. Although the deflection may be a remnant of the initial perturbation due to the high-temperature spark created by the focused laser line, the velocity data suggest it is a weak compression wave traveling with the large-scale structure. Lastly, as the large-scale structure propagated downstream, a decrease in the size of the recirculation region and in the maximum magnitude of the reverse velocities was also observed. This characteristic is most clearly seen by comparing Fig. 7a and Fig. 7f, where the reverse velocities decrease by almost 50% from the unforced case. As a result, in Fig. 7f, the reverse velocities reach roughly 13% of the freestream value ($\sim$55 m/s).

3. *Correlation Parameters*

Another parameter of interest in the current investigation was the convective velocity of the large-scale structure that developed in the shear layer. From this quantity, the convective velocity ratio can be calculated, for which, as noted earlier, choosing an appropriate value has been an unresolved issue in previous studies. Furthermore, the large-scale structure in this investigation was forced in the shear layer as opposed to naturally occurring through the feedback mechanism, which also allows for comparison under these conditions. To quantify and analyze the development of this parameter, the positive and negative transverse velocity regions of each vortex in the shear layer were tracked in space and time. This method was selected as a consequence of the centroid (position of local minimum or maximum transverse velocity) for each region being well defined. Given the associated error in the PIV velocity data and spatial resolution of the images, it was estimated that the centroidal position for each region was calculated with an uncertainty of ± 0.2 mm. Curve fitting of the experimental data also suggested that this estimate was reasonable.

Using the delay time between the excitation pulse and imaging, as well as the relationship between pixels and distance, the experimental convective velocities were determined for each of the four regions. These velocities are related to the inverse of the slope for each of the regions position-time curves as displayed in Fig. 8 and the cavity depth. Again, in Fig. 8, regions I–IV are identified and labeled as in Fig. 5e; the position of the stagnation point between the two vortices seen in Fig. 6 is similarly presented. The data sets of time-related positions have also been fit with linear curves. As can be seen in Fig. 8, to a good approximation, a linear fit can describe all variability in the positions of each set of experimental points. Accordingly, this illustrates that, although the convective velocity varies between each region (I–IV), it remains constant with changes in time and position. These velocities have also been summarized in Table 2. In Table 2, a theoretical value for the convective velocity of the stagnation point has been included. From the work of Papamoschou and Roshko [19], this convective velocity is assumed to represent the entire large-scale structure. The calculation of the theoretical convective velocity listed in Table 2 for the stagnation point was based on the assumption that the effective freestream velocity of the low-speed side was zero in the cavity, and the speed of

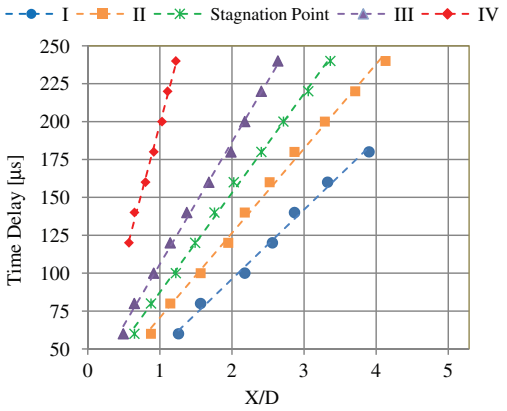

Fig. 8 Spatial tracking of different features of the large-scale structure in time; points represent experimental data and lines as linear fit curves.

sound in the cavity was calculated assuming adiabatic temperature recovery, yielding a value of 224 m/s. This value is slightly higher (8.2%) in comparison to the measured results using the PIV data. However, it is interesting to note that, as the temperature of the fluid in the cavity reduces to the freestream value, the theoretical convective velocity approaches the experimental value of 207 m/s.

There are also several other trends that can be inferred by comparing the different convective velocities in Table 2. In particular, by temporally tracking the positions of regions I–IV and the stagnation point, the convective velocity for the large-scale structure was spatially sampled along its streamwise length. From Table 2 and Fig. 8, beginning with region I, the convective velocity decreased from 297 to 77 m/s for region IV. Therefore, because the convective velocities were also constant in time, this result suggests a linear growth rate, or streamwise stretching, for the large-scale structure.

To further investigate the streamwise and transverse growth rate for the large-scale structure, a characteristic length and height were calculated. In determining this parameter, similar to Fig. 6, the streamlines were plotted in a convective reference frame allowing the core of each vortex to be visualized. Using the coordinates for each origin, the characteristic length was then expressed as the difference in the streamwise locations between the cores of the upstream and downstream vortices. The results are shown in Fig. 9, where the values have been nondimensionalized by the unperturbed local shear layer thickness at the location of the stagnation point for each corresponding delay time. Once the shear layer becomes fully developed, its thickness was expected to grow linearly along the length of the cavity [19]. A characteristic height was also calculated by taking the difference of the vortex core locations in the transverse direction.

In quantifying the accuracy of the values presented in Fig. 9, consideration was given to several sources of error. These included the uncertainty in the convective velocity, shear layer thickness, mean velocity, and in the ability to resolve each vortex core. Based on these factors, the values presented for the characteristic length and height were estimated to be within ±0.3 mm, or approximately ±0.02 in terms of the nondimensional values presented in Fig. 9. In interpreting the data shown in Fig. 9, a linear trend in time appears to exist for the nondimensionalized characteristic length and height

Table 2 Summary of convective velocities

	Convective velocity, m/s	
	Experimental	Theoretical
I	297 ± 9	——
II	242 ± 8	——
Stagnation point	207 ± 7	224
III	169 ± 6	——
IV	77 ± 4	——

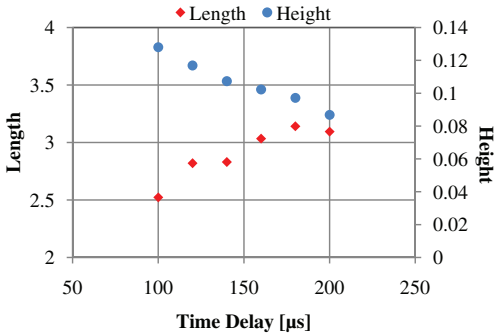

Fig. 9 Characteristic length and height scale nondimensionalized by unperturbed local shear layer thickness.

scales. This result is consistent with the constant convective velocities for regions I–IV of the large-scale structure as shown in Table 2. Additionally, the streamwise distance between the upstream and downstream vortices is increasing at a rate greater than the growth of the shear layer. For the transverse direction, the distance between the vortices is decreasing. However, it is only slightly greater than the uncertainty of the measurement, and it is unclear whether this trend will continue after a value of zero for the characteristic height is achieved.

V. Conclusions

With many applications in aeronautics and other disciplines, the practical interest in the prediction and control of a cavity flowfield has fueled a significant amount of research activity in recent years. Although the studies have differed in their ultimate goal, ranging from suppression or enhancement of fluid dynamic features to a pure investigation of the salient behavior, they all contribute to the further understanding of cavities and their control. In the current investigation, as a means of active flow control, an energy input was applied to the leading edge of an open cavity using a Q-switched Nd:YAG pulsed laser. The experiment was conducted at a freestream Mach number of 1.4 and for a cavity with a length-to-depth ratio of 5.29. With schlieren imaging and two-component measurements, it was determined that the laser energy deposition resulted in the formation of a large-scale structure within the shear layer. The underlying composition and behavior of this forced structure were revealed with velocity vector field data. Specifically, these measurements were used to compute an experimental convective velocity, which were in good agreement, although slightly lower than predicted values of a theoretical model proposed by past researchers. Although the findings in this study are particularly attractive for applications where it is desired to effectively bring together fluid in the cavity with the freestream fluid, further investigation is needed to confirm adaptability to other flowfield conditions.

Acknowledgments

The authors would like to thank the U.S. Air Force Office of Scientific Research with John Schmisseur for funding this work on energy deposition using laser-induced optical breakdown (FA9550-07-0215). Any opinions, findings and conclusions, or recommendations expressed in the material are those of the authors and do not necessarily reflect the views of the U.S. Air Force Office of Scientific Research. Additionally, we would like to thank our colleagues Doyle Knight, Graham Candler, and Hong Yan for their discussions and input regarding this work.

References

[1] Zhang, X., "Compressible Cavity Flow Oscillation due to Shear Layer Instabilities and Pressure Feedback," *AIAA Journal*, Vol. 33, No. 8, 1995, pp. 1404–1411.
doi:10.2514/3.12845

[2] Zhang, J., Morishita, E., Okunuki, T., and Itoh, H., "Experimental and Computational Investigation of Supersonic Cavity Flows," AIAA Paper 2001-1755, 2001.
[3] Zhuang, N., Alvi, F. S., Alkislar, M. B., Shih, C., Sahoo, D., and Annaswamy, A. M., "Aeroacoustic Properties of Supersonic Cavity Flows and Their Control," AIAA Paper 2003-3101, 2003.
[4] Perng, S. W., and Dolling, D. S., "Suppression of Pressure Oscillations in High-Mach-Number, Turbulent, Cavity Flow," *Journal of Aircraft*, Vol. 38, No. 2, 2001, pp. 248–256. doi:10.2514/2.2782
[5] Sinha, N., Arunajatesan, S., Shipman, J., and Seiner, J. M., "High Fidelity Simulation and Measurements of Aircraft Weapons Bay Dynamics," AIAA Paper 2001-2125, 2001.
[6] Aradag, S. S., Yan, H., and Knight, D., "Energy Deposition in Supersonic Cavity Flow," AIAA Paper 2004-514, 2004.
[7] Rizzetta, D. P., and Visbal, M. R., "Large-Eddy Simulation of Supersonic Cavity Flowfields Including Flow Control," *AIAA Journal*, Vol. 41, No. 8, 2003, pp. 1452–1462. doi:10.2514/2.2128
[8] Unalmis, O. H., Clemens, N. T., and Dolling, D. S., "Cavity Oscillation Mechanisms in High-Speed Flows," *AIAA Journal*, Vol. 42, No. 10, 2004, pp. 2035–2041. doi:10.2514/1.1000
[9] Nichols, R. H., and Westmoreland, S., "Comparison of CFD Approaches for Simulating Flow Inside a Weapons Bay," AIAA Paper 2006-455, 2006.
[10] Kim, C.-K., Yu, S.-T. J., and Zhang, Z.-C., "Cavity Flow in Scramjet Engine by Space–Time Conservation and Solution Element Method," *AIAA Journal*, Vol. 42, No. 5, 2004, pp. 912–919. doi:10.2514/1.9017
[11] Yu, K. H., Wilson, K. J., and Schadow, K. C., "Effect of Flame-Holding Cavities on Supersonic-Combustion Performance," *Journal of Propulsion and Power*, Vol. 17, No. 6, 2001, pp. 1287–1295. doi:10.2514/2.5877
[12] Ben-Yakar, A., and Hanson, R. K., "Cavity Flame-Holders in Ignition and Flame Stabilization in Scramjets: An Overview," *Journal of Propulsion and Power*, Vol. 17, No. 4, 2001, pp. 869–877. doi:10.2514/2.5818
[13] Murray, R. C., and Elliott, G. S., "Characteristics of the Compressible Shear Layer over a Cavity," *AIAA Journal*, Vol. 39, No. 5, May 2001, pp. 846–856. doi:10.2514/2.1388
[14] Quick, A., King, P. I.Gruber, M. R., Carter, C. D., and Hsu, K.-Yu, "Upstream Mixing Cavity Coupled with a Downstream Flameholding Cavity Behavior in Supersonic Flow," AIAA Paper 2005-3709, 2005.
[15] Rossiter, J. E., "Wind Tunnel Experiments on the Flow over Rectangular Cavities at Subsonic and Transonic Speeds," Aeronautical Research Council, Repts. and Memoranda No. 3488, London, Oct. 1964.
[16] Heller, H. H., and Bliss, D. B., "The Physical Mechanism of Flow-Induced Pressure Fluctuations in Cavities and Concepts for Their Suppression," AIAA Paper 75-491, March 1975.
[17] Brown, G., and Roshko, A., "On Density Effects and Large Structure in the Turbulent Mixing Layers," *Journal of Fluid Mechanics*, Vol. 64, No. 4, 1974, pp. 775–816. doi:10.1017/S002211207400190X
[18] Smits, A. J., and Dussauge, J. P., "Introduction," *Turbulent Shear Layers in Supersonic Flow*, 2nd ed., Springer, New York, 2005, pp. 15–17.
[19] Papamoschou, D., and Roshko, A., "The Compressible Turbulent Shear Layer: An Experimental Study," *Journal of Fluid Mechanics*, Vol. 197, 1988, pp. 453–477. doi:10.1017/S0022112088003325
[20] Island, T. C., Urban, W. D., Mungal, M. G., "Mixing Enhancements in Compressible Shear Layers via Sub-Boundary Layer Disturbances," *Physics of Fluids*, Vol. 10, No. 4, 1998, pp. 1008–1020. doi:10.1063/1.869620
[21] Cattafesta, L. N., Williams, D. R., Rowley, C. W., and Alvi, F. S., "Review of Active Control of Flow-Induced Cavity Resonance," AIAA Paper 2003-3567, 2003.
[22] Adelgren, R. G., Elliott, G. S., and Crawford, J. B., "Axisymmetric Jet Shear-Layer Excitation by Laser Energy and Electric Arc Discharges," *AIAA Journal*, Vol. 43, No. 4, 2005, pp. 776–791. doi:10.2514/1.8548
[23] Zhuang, N., Alvi, F. S., Alkislar, M. B., and Shih, C., "Supersonic Cavity Flows and Their Control," *AIAA Journal*, Vol. 44, No. 9, 2006, pp. 2118–2128. doi:10.2514/1.14879
[24] Chan, S., Zhang, X., and Gabriel, S., "Attenuation of Low-Speed Flow-Induced Cavity Tones Using Plasma Actuators," *AIAA Journal*, Vol. 45, No. 7, 2007, pp. 1525–1538. doi:10.2514/1.26645
[25] Knight, D., "Survey of Aerodynamic Flow Control at High Speed by Energy Deposition," AIAA Paper 2003-525, 2003.
[26] Swanson, T., "Interaction of Laser Energy Deposition with a Normal Shock," M.S. Thesis, Univ. of Illinois Urbana–Champaign, Urbana, IL, 2006.
[27] Martens, S., Kinzie, K. W., and McLaughlin, D. K., "Measurements of Kelvin-Helmholtz Instabilities in a Supersonic Shear Layer," *AIAA Journal*, Vol. 32, No. 8, 1994, pp. 1633–1639. doi:10.2514/3.12153
[28] Sandham, N. D., and Reynolds, W. C., "Compressible Mixing Layer: Linear Theory and Direct Simulation," *AIAA Journal*, Vol. 28, No. 4, 1990, pp. 618–624. doi:10.2514/3.10437
[29] Clemens, N. T., and Mungal, M. G., "Two- and Three- Dimensional Effects in the Supersonic Mixing Layer," *AIAA Journal*, Vol. 30, No. 4, 1992, pp. 973–981. doi:10.2514/3.11016
[30] Humphreys, W. M., Jr., and Bartram, S. M., "Measurement of Separating Flow Structures Using a Multiple-Camera DPIV System," *19th International Congress on Instrumentation in Aerospace Simulation Facilities*, Inst. of Electrical and Electronics Engineers, New York, 2001, pp. 82–93.
[31] Urban, W. D., and Mungal, M. G., "Planar Velocity Measurements in Compressible Mixing Layers," *Journal of Fluid Mechanics*, Vol. 431, 2001, pp. 189–222. doi:10.1017/S0022112000003177
[32] Huffman, R., "An Experimental Investigation into the Effect of Plasma on the Flow Features of an Axisymmetric Jet," Ph.D Dissertation, Univ. of Illinois Urbana–Champaign, Urbana, IL, 2006.
[33] Scarano, F., and van Oudheusden, B. W., "Planar Velocity Measurements of a Two-dimensional Compressible Wake," *Experiments in Fluids*, Vol. 34, No. 3, March 2003, pp. 430–441. doi:10.1007/s00348-002-0581-x
[34] Melling, A., "Seeding Gas Flows for Laser Anemometry," *AGARD Conference Proceedings*, No. 399, 1986, pp. 8.1–8.11.
[35] Samimy, M., and Lele, S. K., "Motion of Particles with Inertia in a Compressible Free Shear Layer," *Physics of Fluids*, Vol. 3, No. 8, 1991, pp. 1915–1923. doi:10.1063/1.857921
[36] Herrin, J. L., and Dutton, J. C., "Effect of a Rapid Expansion on the Development of Compressible Free Shear Layers," *Physics of Fluids*, Vol. 7, No. 1, 1995, pp. 159–171. doi:10.1063/1.868737
[37] Adrian, R. J., and Christensen, K. T., and Liu, Z.-C., "Analysis and Interpretation of Instantaneous Turbulent Velocity Field," *Experiments in Fluids*, Vol. 29, No. 3, 2000, pp. 275–290. doi:10.1007/s003489900087
[38] Kline, S. J., and Robinson, S. K., "Quasi-Coherent Structures in the Turbulent Boundary Layer, Part I: Status Report on a Community-Wide Summary of the Data," *Proceedings of Zaric Memorial Conference*, Hemisphere, New York, 1990, pp. 200–217.

N. Clemens
Associate Editor